Pressure drop analysis of oscillating flows through a miniature porous regenerator under isothermal and nonisothermal conditions

Emna Dellali, Sylvie Bégot, François Lanzetta, Eric Gavignet, Jean-Yves Rauch

HAL Id: hal-02131041
https://hal.science/hal-02131041

Pressure drop analysis of oscillating flows through a miniature porous regenerator under isothermal and nonisothermal conditions

E. Dellali[1], S. Bégot[1]*, F. Lanzetta[1], E. Gavignet[1], J.Y Rauch[2]

[1]FEMTO-ST Institute, Univ. Bourgogne Franche-Comté, CNRS, Département ENERGIE, 90000 Belfort, France

[2]FEMTO-ST Institute, Univ. Bourgogne Franche-Comté, CNRS, Département AS2M, 25000 Besançon, France

sylvie.begot@univ-fcomte.fr

Abstract

In this paper, we present an experimental study on the pressure, pressure drop, velocity and friction factor in a regenerator made from an array of pillars in reciprocating flow conditions. The fluid used in the experiment is air. We show that the pressure drop depends on the porosity, frequency and stroke. We observe a phase shift between the crank angle sinusoidal variation of the piston and the pressure variation that increases with frequency. We also observe that the instantaneous friction factor is higher in the discharge phase than in the suction phase, and higher in the acceleration than in the deceleration phase. Friction factor in oscillating flow appears to be higher than friction factor in steady unidirectional flow for the highest porosity. For the lower porosities, we observe that the pressure drop and friction factors are similar for maximum Reynolds numbers lower than 5000. An experimental correlation for the friction factor of the regenerator is derived in order to design a millimetric Stirling engine. The friction factor is compared with friction factors reported for woven screens, metal felts and involute foil regenerators.

Highlights

- New Stirling millimetric engine regenerator made from arrays of pillars
- Pressure, pressure drop and velocity experimental results
- Comparison between unidirectional and reciprocating flows
- New friction factor experimental correlation

Keywords: Stirling engine, regenerator, reciprocating flow, pressure drop, friction factor, millimetric size

Nomenclature

C stroke [mm]

D diameter [mm]

e thickness [mm]

f friction factor

$freq$ frequency [Hz]

h height [mm]

k coverage factor

L length [mm]

n number of observations

P pressure [bar]

Re Reynolds number

Re_ω kinetic Reynolds number $\frac{\omega D_h^2}{\nu}$

S surface [mm²]

SF shape factor

u velocity [m.s⁻¹]

V volume [mm³]

Va Valensi number $\frac{\omega D_h^2}{4\nu}$

X observation

x fluid displacement [mm]

z uncertainty

Z expanded uncertainty

Greek

ε porosity

ρ fluid density [kg.m⁻³]

$??$ fluid kinematic viscosity [m².s⁻¹]

ω angular frequency [rad.s⁻¹]

Subscripts

acc acceleration

C cold

dec deceleration

H hot

h hydraulic diameter

p pillar

1 Introduction

Interest in Stirling engines has grown recently because they can work with many heat sources including combustion of biofuels, solar sources or waste heat. Recovering waste heat at low temperature can lead to design miniaturized Stirling engines, therefore changing fabrication technology and move to 3D printing or clean room fabrication [1][2]. Whatever the machine size, the regenerator in Stirling engine is a key element because the engine efficiency is strongly dependent on its thermal and fluidic performances [3]. The regenerator is a porous medium subjected to reciprocating flows between the hot source and the cold sink. Therefore, fluidic performances in reciprocating flows have to be known to design efficient Stirling engines, although most of the published correlation concerns unidirectional steady flows.

In most present engines, the regenerator consists of woven screen packed columns. One of the first values for pressure drops in woven screens regenerators was given by Kays and London [4] who obtained them from steady unidirectional flows experiments. Later, Miyabe *et al*. [5] proposed more experimental correlations in steady flows. This correlation and those reported by others authors are summarized in the Table 1 which is an update of the table published by Xiao *et al.* [6]. Studies that are more recent propose experimental correlations for regenerators under reciprocating flows and compare their results with those achieved in steady flows. Tanaka *et al*. [7] obtained instantaneous pressure drops and friction factors versus Reynolds number for different materials. They reported oscillating pressure drops higher than unidirectional pressure drops. Gedeon and Wood [8] have also studied the pressure drop within manufactured regenerators made of woven screens or metal felts. They did not find any significant differences between steady and oscillating type's flows, except at Valensi numbers higher than 20. Zhao and Cheng [9] have studied the pressure drop for a woven screen regenerator and expressed the friction factor as a function of the dimensionless fluid displacement and the kinetic Reynolds number. They found that the pressure drop could be 4 and 6 times larger than the pressure drop in steady flow computed from Miyabe's correlation. Hsu *et al*. [10] studied the pressure drop in a regenerator formed by wire screens in steady and oscillating flows. They have shown that the pressure drop coefficient is identical to the steady flow for Reynolds numbers between 1 and 2000. They stated that the oscillating flows seems to behave as quasi-steady for frequencies lower than 4 Hz. Wang *et al*. experimentally investigated the friction factor in oscillating flow for frequencies of 30 Hz, 40 Hz, 50 Hz and 60 Hz [11]. They compared their measurements to Miyabe *et al*. [5] correlation and reported an increase in oscillating flows from 2 to 4. Leong and Jin [12] have studied the pressure drop for open-cell metal foam regenerators in oscillating flows. The results showed that the flow is governed by a hydraulic ligament diameter based kinetic Reynolds number. They reported a much smaller friction factor in the foam than in wire screens. Ibrahim *et al*. [13] studied the effect of complex geometry inserts in a channel for oscillating fluid flow for different frequencies and displacements. The pressure drop was shown to be mainly due to gas inertia for the case of rectangular duct with no insert. With inserts, they stated that the pressure drop has three sources: inertia, friction and local losses. They also observed that the dimensionless pressure drop decreases with increasing kinetic Reynolds number. Later, they proposed an involute foil regenerator and measured friction factors [14]. Sun *et al*. studied involute foil geometries at a larger scale and proposed friction factors correlations [15]. Mitchell *et al*. [16] led work on micro-manufactured regenerators in etched silicon sheets and observed friction factors substantially lower than those observed for screens and spheres. Pamuk and Özdemir [17] carried on studies on a regenerator formed by stacks of steel balls and established a correlation that defines the friction factor. They have showed that a 6% increase in porosity smooth the difference in terms of losses load between oscillating and permanent flows.

Kahaleras *et al*. [18] conducted experiments on regenerators manufactured by selective laser melting and consisting of metallic mini-channels of different geometries and low porosities (30%, 35% and 40 %). They proposed friction factors for their designed regenerators. Xiao *et al*. [6] conducted experimental studies for steady and oscillating flow within a woven screen regenerator. They showed that the correlations established in case of steady state are always applicable for a range of small kinetic Reynolds numbers depending on the number of the screens.

To conclude on the first part of this review, we observe that the published works on woven screens or micro and mini-channel regenerators in reciprocating flows are not in accordance concerning the impact of the oscillating flow compared to unidirectional flow.

On another note, arrays of pillars or pin fins heat exchangers can be an alternative to woven screens regenerators. Pin fins exchangers have been studied and developed for various applications including heat dissipation of microprocessors [19], micro reactors [20][21][22] or active magnetic regeneration [23]. Correlations for pressure drop at steady sate and unidirectional flow were established. In order to enhance the performance of micro cryocoolers, Vanapalli *et al.* [24] investigated the pressure drop of steady unidirectional gas flows in a microchannel filled with a dense pillar matrix. They studied different pillar shapes, aligned or staggered patterns and obtained experimental results for friction factors for Reynolds numbers in the range of 50–500. A comparison of friction factor correlations for circular pillar cross-sections agreed rather well with the correlations proposed for the macroscale. In oscillating flows, experimental results are scarce: Jeng *et al.* [25] performed flow visualization and heat transfer analysis of a pin-fin heat sink submitted to an oscillating airflow, but no analysis of pressure or pressure drop were made.

To conclude on the second part of this review, we observe that no experimental results are available on pressure drop analysis for regenerators made from arrays of pillars in oscillating flow.

In this work, we present a new geometry for a regenerator based on arrays of pillars in a rectangular mini channel for a millimetric Stirling engine. We present new experimental results in pressure, velocity, pressure drop and friction coefficient in reciprocating airflow. We conclude by establishing a new correlation for the friction factor and a comparison with friction factors reported for other technologies of regenerators.

The first part of the paper introduces the regenerator design and fabrication. The second part describes the experimental apparatus and uncertainty analysis. The third part presents experimental results.

Authors	Regenerator geometry	Correlation	Conditions	Fluid	Comparison with steady and unidirectional flow
Miyabe *et al.* 1958 [5]	Woven screens	$f = \dfrac{33.6}{Re_l} + 0.0337$ Unidirectional steady flow	$0.586 < \varepsilon < 0.840$ $5 < Re_{dl} < 1000$ $f = \dfrac{\Delta P}{n} / (1/2\rho u^2)$ dl: mesh distance, n: number of screens	N$_2$	
Tanaka *et al.* 1990 [7]	Woven screens Sponge metal Sintered metal	$f_h = \dfrac{175}{Re_h} + 1.6$	Woven screens $0.645 < \varepsilon < 0.729$; sponge metal $0.702 < \varepsilon < 0.956$; sintered : $\varepsilon = 0.372$ $10 < Re_h < 2000$ $Re_h = \dfrac{u_{max}D_h}{\nu}$ freq: $1.67 - 10\ Hz$ $f_h = \Delta P D_h / (1/2\rho u_{max}^2 L)$ $D_h = \dfrac{\varepsilon D_w}{(1-\varepsilon)}$ D_w : wire diameter	Air	For most of the results : $f_{oscillating} > f_{steady}$ Raise of 30% measured in pipe bundle
Zhao *and* Cheng 1995 [9]	Woven screens	$f_{max} = \dfrac{1}{(A_0)_h}\left[\dfrac{403.2}{(Re_\omega)_h} + 1789.1\right]$ $\bar{f} = \dfrac{1}{(A_0)_{Dh}}\left[\dfrac{247.3}{(Re_\omega)_h} + 1003.6\right]$	$0.01 < (Re_\omega)_h < 0.13$ $0.602 < \varepsilon < 0.662$ freq: $2 - 56\ Hz$ $(Re_\omega)_h = \dfrac{\omega D_h^2}{\nu}$ $D_h = \dfrac{\varepsilon D_w}{(1-\varepsilon)}$ $(A_0)_{dh} = \dfrac{x_{p,max}}{D_h}$ D_w : wire diameter	Air	The cycle averaged friction factor is 4 to 6 times higher than the friction factor issued from the steady flow friction factor issued from Miyabe's correlation
Gedeon and Wood 1996 [8]	Woven screens Metal felts	$f = \dfrac{129}{Re} + 2.91Re^{-0.103}$ $f = \dfrac{192}{Re} + 4.35Re^{-0.067}$	$0.6232 < \varepsilon < 0.7102$; $0.45 < Re < 6100$; $0.052 < Va < 21$; $0.688 < \varepsilon < 0.8405$; $0.11 < Re < 2500$; $0.021 < Va < 5.6$;	N$_2$, He	No significant difference if $Va < 20$
Hsu *et al.* 1999 [10]	Woven screens	$f = \dfrac{109.3}{Re_h} + \dfrac{5}{Re_h^{1/2}} + 1$	$0.7 < \varepsilon < 0.8$ $0.27 < Re_h < 2600$ $Re_h = \dfrac{u_{max}D_h^2}{\nu}$ $f_{max} = \Delta P_{max} D_h / (1/2\rho u_{max}^2 L_r)$ $D_h = \dfrac{\varepsilon D_w}{(1-\varepsilon)}$	Air	No difference if $freq < 4\ Hz$
Wang *et al.* 2004 [11]	Woven screens		freq: $30 - 60\ Hz$	Air	For high frequency, the friction factor deviates significantly from that for steady flow (2 to 4.5 times at 50 Hz). Comparison is made from Miyabe's correlation

Leong and Jin 2006 [12]	Open-cell metal foam	$f_{max} = \dfrac{1}{A_{Dh}}\left[\dfrac{86.7}{(Re_{\omega})_h^{0.19}} + 0.61\right]$		$\varepsilon = 0.9$ $0.46 < (Re_{\omega})_h < 57.9$ $(Re_{\omega})_h = \dfrac{\omega D_h^2}{\nu}$ $freq: 1 - 10\ Hz$ ==$f_{max} = \Delta P_{max} D_h / (1/2\rho u_{max}^2 L)$== $D_h = \dfrac{\varepsilon D_l}{(1-\varepsilon)}$ $A_{Dh} = \dfrac{x_{max}}{D_h}$ ==D_l : ligament diameter of the foam==	Air	No comparison of steady and unidirectional flow Comparison of metal foam to woven screen
Ibrahim *et al.* 2007 [14]	Involute foil	$f = \dfrac{117.3}{Re_h} + 0.38 Re_h^{-0.053}$		$0.7 < \varepsilon < 0.8$ $3.4 < Re_h < 1190$ $0.11 < Va < 3.8$	N_2, He	Pressure drops increase with increasing Reynolds number Dimensionless pressure drops decrease with increasing kinetic Reynolds number
Sun *et al.* 2009 [15]	Involute foil	$f = \dfrac{153.1}{Re_h} + 0.127 Re_h^{-0.01}$		$\varepsilon = 0.84$ $132 < Re_h < 2350$		No comparison
Pamuk and Özdemir 2012 [17]	Packed steel balls (water)	$f_{max} = \dfrac{3083998}{A_0 Re_{\omega}/2} + 1882$		$0.37 < \varepsilon < 0.4$ $500 < Re_{max} < 6800$ $Re_{max} = A_0 Re_{\omega}/2$ $freq: 0.116 - 0.35\ Hz$ $f_{max} = \Delta P D_i / (1/2\rho u^2 L)$ $A_0 = \dfrac{x_{max}}{D_i}$	Water	One medium : no significant difference Second medium : ==$f_{oscillating} > f_{steady}$==
Kahaleras *et al.* [18]	Sintered metals channels	$f = \dfrac{0.00689}{Re_{\omega}} + 0.791$ $f = \dfrac{0.00279}{Re_{\omega}} + 0.00186$ $f = \dfrac{0.00246}{Re_{\omega}} + 0.02962$	$\varepsilon = 0.3$; Pyramidal mesh; $D_h = 0.178\ mm$; $0.005 < Re_{\omega} < 0.075$ $\varepsilon = 0.35$; Straight mesh; $D_h = 0.237\ mm$; $0.01 < Re_{\omega} < 0.13$ $\varepsilon = 0.40$; Straight mesh; $D_h = 0.250\ mm$; $0.01 < Re_{\omega} < 0.15$ $freq: 1 - 6\ Hz$		Air	No comparison
Xiao *et al.* 2017 [6]	Woven screens	$f = \dfrac{134}{Re_h} + 5.44 Re_h^{-0.188}$		$0.665 < \varepsilon < 0.78$ $2.59 \times 10^{-2} < Re_{\omega} < 2.04 \times 10^{-1}$ (100 mesh) $6.60 \times 10^{-3} < Re_{\omega} < 5.52 \times 10^{-2}$ (300 mesh) $1.43 \times 10^{-3} < Re_{\omega} < 1.13 \times 10^{-2}$ (400 mesh) $Re_h = \dfrac{u D_h^2}{\nu}$ $D_h = \dfrac{\varepsilon D_w}{(1-\varepsilon)}$ ==D_w : wire diameter==	Air	Same correlation can be applied within this range of experiment

Table 1. Correlations for the friction factors

2 Regenerator under analysis

2.1 Regenerator model

Rühlich and Quack [26] showed by using Computational Fluid Dynamics (CFD) that the optimum geometry for regenerators made from arrays of pillars consists of slim elements in the flow direction in a staggered overlapping arrangement. Therefore, the regenerator was designed as an array of pillars included in a rectangular channel of 5x2.5 mm^2 cross section and 60 mm length (Figure 1). The channel total volume V is 750 mm^3. The pillars are eye-shaped and staggered inside the channel with three different porosities: 0.8, 0.85 and 0.9 (Figure 2 and Table 2). The surface and volume of this matrix are denoted as S_{matrix} and V_{matrix}. Following the definition used by Rühlich *et al.* [26], the porosity ε is defined as:

$$\epsilon = 1 - \frac{V_{matrix}}{V} \qquad (1)$$

The hydraulic diameter is calculated as:

$$D_h = \frac{4\varepsilon V}{S_{matrix}} \qquad (2)$$

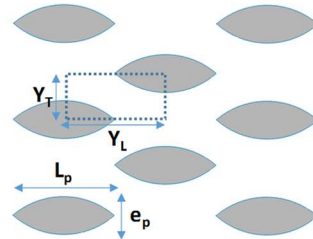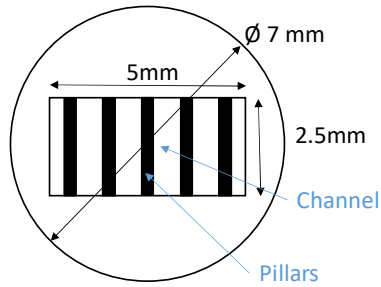and the shape factor is defined as [12]:

$$SF = \frac{e_p}{L_p} \qquad (3)$$

Figure 1: Regenerator cross section   *Figure 2: Pillars shape and staggered arrangement*

Pillar dimensions (mm)	Shape factor	Porosity ε	Arrangement dimensions (mm)	Hydraulic diameter D_h (mm)
e_p = 0.62 L_p = 1.24 h_p = 2.5	0.5	0.8	Y_L = 1.24 Y_T = 1.24	2.1
		0.85	Y_T = 1.24 Y_L = 2.24	2.5
		0.9	Y_T = 1.24 Y_L = 2.51	3.7

Table 2. Staggered pillars dimensions and layout

Referring to the classification of Kandlikar and Grande [27], the regenerator with a 90% porosity is a conventional channel while the others can be considered as mini channels, because the hydraulic diameter is lower than 3 mm.

In the next paragraphs, the analysis of the experimental regenerator performance is made using the maximum Reynolds number $Re_{D_h,max}$. It is defined as the Reynolds number based on the hydraulic diameter and the maximum velocity observed over the cycle:

$$Re_{D_h,max} = \frac{u_{max}D_h}{\nu} \tag{4}$$

The maximum velocity u_{max} is defined as the maximum free stream velocity u_∞ observed over a cycle divided by the porosity:

$$u_{max} = \frac{u_{\infty,max}}{\varepsilon} \tag{5}$$

The friction factor is analyzed during the cycle by the instantaneous friction factor f for a reciprocating flow of an incompressible fluid within the regenerator [11]:

$$f\big(t, u(t), du/dt(t)\big) = \frac{\Delta p(t)D_h}{\frac{1}{2}\rho u^2(t)L} - \left[\frac{D_h}{u^2(t)}\left(\frac{du}{dt}\right)\right] \tag{6}$$

where the second term on the right hand side accounts for inertial effects. If the inertial effects are negligible, this expression reduces to:

$$f\big(t, u(t)\big) = \frac{\Delta p(t)D_h}{\frac{1}{2}\rho u^2(t)L} \tag{7}$$

The maximum friction factor is determined using the maximum pressure drop value and the maximum velocity observed over a cycle:

$$f_{max} = \frac{\Delta p_{max}D_h}{\frac{1}{2}\rho u_{max}^2 L} \tag{8}$$

2.2 Fabrication

The regenerator was made by an additive manufacturing process. The manufacturing process used is Multiple Jet Molding and the 3D printer is a printer ProJet™ HD 3500. The laminating pitch is 0.2 mm. The thickness of the layers deposited is 32 μm for a resolution of 375 x 375 x 790 DPI (X Y Z). The typical precision of the machine is of the order of 0.1 - 0.2% of the dimensions of the printed object. The material used for the preparation of the regenerator is a UV-curable acrylate polymer of the type "Visijet 39 Crystal ". The thermophysical properties of the regenerator material are presented in the Table 3. An example of the regenerator is presented in Figure 3. From the outside, the regenerator is a cylinder. Inside, a rectangular channel with a matrix of pillars runs through.

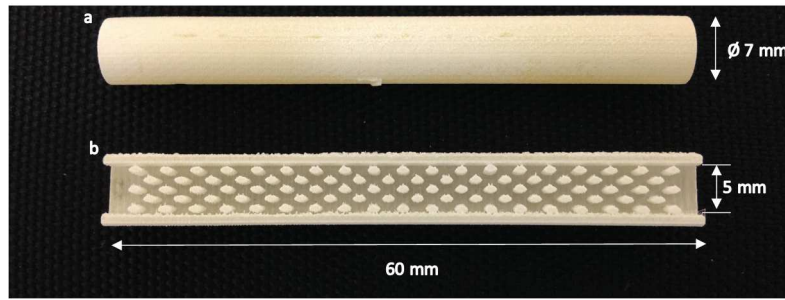| ρ (kg.m^{-3})	λ (W.m^{-1}.K^{-1})	C_P (J.kg^{-1}.K^{-1})	α (m^2.s^{-1})	b (J.K^{-1}m^{-2}.s$^{-1/2}$)
1064	0.216	1670	1.22×10^{-7}	620

Table 3 : Thermophysical properties of the regenerator

Figure 3 : Regenerator under analysis. ε = 0.8. a/ outside view b/ sectional view

3 Experimental setup

The regenerators were mainly tested in a reciprocating flow, however a comparison at steady state and unidirectional flow was also made. The fluid used in the experiment is air. Both test benches and instrumentation are presented below.

3.1 Test benches and instrumentation

3.1.1 Steady state unidirectional flow test bench

The test bench scheme of the regenerator in unidirectional flow is shown in Figure 4. The air supply comes from a compressor. A rotameter (range 4-50 l/min, Pmax 6.9 bar) with a needle valve enables the measurement of the flow rate. Two pressure transducers (Kulite XCQ-055 1.7 BARA-8068) measure the upstream pressure of the regenerator and the atmospheric pressure at the exhaust.
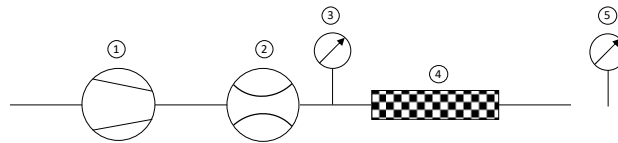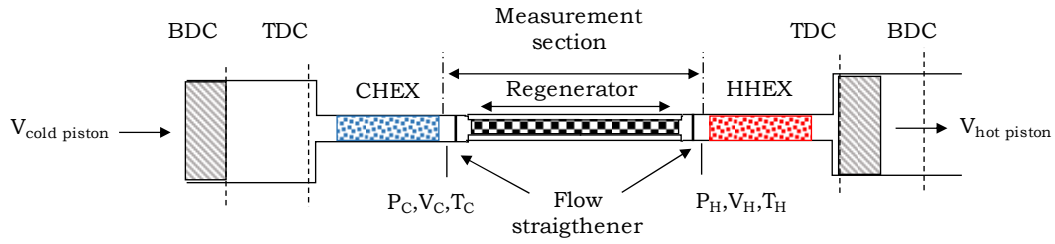

Figure 4 : Experimental scheme for steady flows. 1: compressor, 2: flowmeter, 3: pressure sensor, 4: regenerator, 5: atmospheric pressure sensor

3.1.2 Reciprocating flow test bench

Two pistons mechanically coupled with a phase angle of 180° produce the reciprocating flow (Figure 5 and Figure 6). Two heat exchangers can heat (HHEX) or cool (CHEX) the flow at both ends of the measurement section. The pressure, velocity and temperature of the airflow are measured at both ends of the test section. Flow straighteners that consist of one woven screen are also included. The diameter of the connecting pipes between the heat exchangers and the regenerator is 5 mm.

The ultraminiature pressure transducers are Kulite XCQ-055 1.7 BARA-8068, their bandwidth is 210 kHz. They were calibrated using a Druck PV621 Pressure Station. The velocity measurement is achieved with a hot wire anemometry method (TSI IFA300 range 0.15 – 200 m/s, 600 kHz bandwidth). The probe measures the axial velocity component and was calibrated in the laboratory. The fluid temperatures are measured with in-house 12.7 µm diameter type K microthermocouples (accuracy +/-0.1°C and cut-off frequency 30 Hz) [28]. They were calibrated in the laboratory with a portable calibration oven (550 Gemini LRI), a Pt100 platinum reference probe (accuracy +/- 0.005 °C) and a reference thermometer (PHP 601).

The reference crank angle is set to 0° when the cold side piston is at its Bottom Dead Centre (BDC) and the hot side piston at its Top Dead Centre (TDC).

Figure 5 : Experimental scheme for reciprocating flows – Crank angle at 0°.
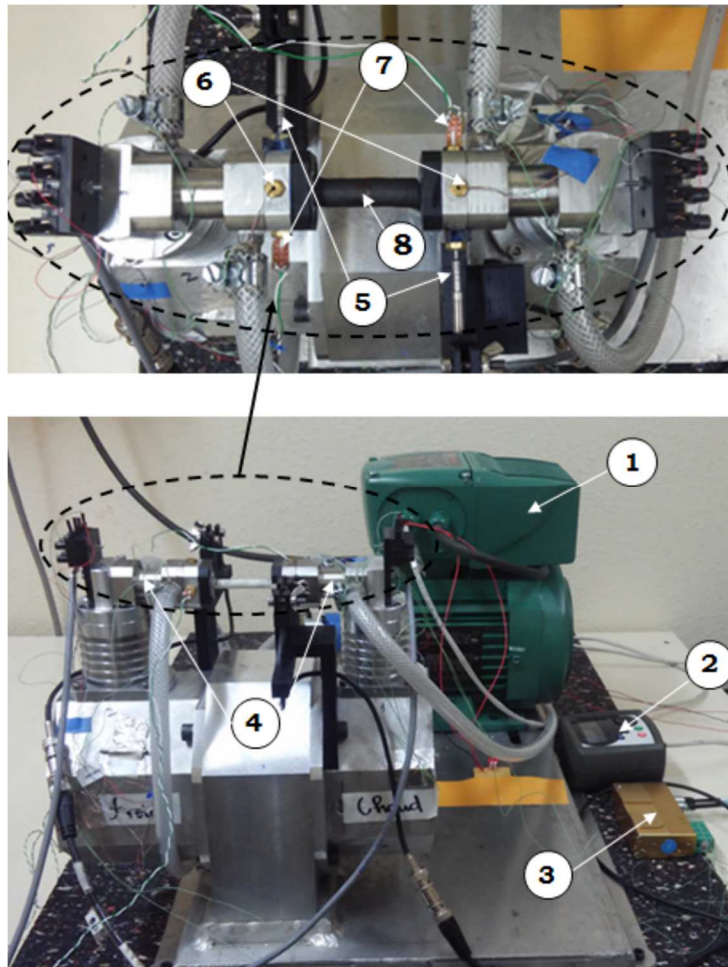
Figure 6 : Test bench 1: electric motor, 2: motor control, 3: thermocouples conditioner, 4: heat exchangers, 5: hot wire anemometer probes, 6: pressure sensors, 7: microthermocouples, 8: regenerator under test

3.2 Uncertainties

The uncertainty analysis was done in accordance with the methodology presented in the Guide to the expression of Uncertainty in Measurement (GUM) [29].

The experimental uncertainty of a quantity X estimated by n independent observations X_i is given in the following (type A uncertainty):

$$z_A = \frac{1}{\sqrt{n}}\left[\frac{1}{n-1}\sum(X_i - \bar{X})^2\right]^{1/2} \quad (9)$$

The pressure and velocity measurement are the average of 40 successive cycles. The maximum type A uncertainties are observed at the lowest frequency (2Hz), they were of 0.022 m.s^{-1} or 1.45% for the maximum velocity at this frequency and 8.75x10^{-5} bar or 1.48% for the maximum pressure drop at this frequency. This worst-case uncertainty is used in the calculation of the total uncertainty.

For the type B uncertainties, we use the supplier characteristics of the calibration apparatus for the velocity and pressure (resp. +/-2% and +/-2.5x10^{-4} bar). We suppose these intervals represent a uniform distribution between the value *[-a, +a]*. Therefore, the type B uncertainty is obtained from:

$$z_B = \frac{a}{\sqrt{3}} \quad (10)$$

The total uncertainty is:

$$z = \sqrt{z_A^2 + z_B^2}$$

The expanded uncertainty is computed as:

$$Z = kz \quad (11)$$

with a coverage factor $k = 2$ corresponding to a 95% confidence interval.

The total relative uncertainty of the velocity varies from 3.7 % at 2 Hz to 2.4% at 10 Hz. The relative pressure uncertainty varies from 5.7 % at 2 Hz to 3.9 % at 10 Hz.

The temperature sensor are calibrated with a reference probe and the uncertainty is 0.1°C. Therefore, the uncertainty among the thermophysical properties due to the uncertainty of the temperature measurement is small compared to the other uncertainties.

The dimensional uncertainties are 0.2% due to the resolution of the 3D printer. The porosity uncertainty is assumed to be 1%.

We suppose that the errors are uncorrelated. Therefore, applying the law of propagation of uncertainties leads to relative uncertainties for the Reynolds number, pressure drop and friction factor. The relative uncertainties depending on the frequency vary from 3.7% to 2.6% for the Reynolds number, from 5.7 to 0.4% for the pressure drop, and for the friction factor, from 7.8% to 3.6%. These uncertainties are reported as error bars in the friction factor graph (cf §4.4).

4 Results and discussion

4.1 Isothermal oscillating flow: pressure and velocity measurements

We first conducted the reciprocating flow experiments through an empty regenerator with no pillars (ε=1), then we conducted experiments with regenerators of three porosities (0.8, 0.85, 0.9). These

tests were made for five frequencies: 2, 4, 6, 8 and 10 Hz (Table 4), and two pistons strokes (24 and 30 mm). The kinetic Reynolds number Re_ω varies from 3.6 to 18.2. The pressure signals at both inlets are plotted versus the piston crank angle in Figure 7 for an empty regenerator (ε=1) and in Figure 8 for a lower porosity (ε=0.8). For an empty regenerator (Figure 7), we observe two maximum values and two minimum values regardless of the piston frequency. Therefore, the pressure signals oscillate at a frequency that is about twice the piston frequency. Moreover, the signal is not completely symmetric about the 180° angle. For a regenerator with a lower porosity (Figure 7), we also observe that the pressure signal frequency is twice the piston frequency at low frequency (freq = 2Hz) and that the pressure signal is asymmetric. This pressure evolution differs from the evolution expected with 2 pistons moving with perfect sinusoidal motion in opposition of phase [30]. Ibrahim *et al.* [13] also reported these observations. Following their interpretation, we suppose that this may be due to the fact that the pistons motions are not perfectly sinusoidal, therefore, the volume of the test section changes slightly. Moreover, the phase difference of the pistons may also differ slightly from 180° leading to the asymmetry of the curves. For a regenerator with a porosity of 0.8, one of the pressure signal maximum raises in amplitude and shifts to smaller crank angles with the increase in the piston frequency up to 10 Hz (Figure 8). At 10 Hz, the pressure signals appear to have the same frequency as the piston but with a strong harmonic content. We also observe a phase angle of about 180° between the inlets. It shows the gas transfer between two sides. As the frequency raises, for a regenerator with a porosity of 0.8, viscous, inertial effects and minor pressure losses are the main contributors of the pressure evolution.

Porosity ε	Stroke C (mm)	Freq (Hz)	Re_ω	Va	$Re_{dh,max}$	Thermal condition T_H (°C) ; T_C (°C)
0.8			3.6 - 18.2	0.9-4.6	935-4141	Isothermal 22°C
						45 ; 15
						55 ; 15
				0.8-4.1	800-3857	65 ; 15
0.85			5.2-26	1.3-6.5	981-5252	Isothermal 22°C
	24 ; 30	2 - 10				45 ; 15
						55 ; 15
			4.8-18.4	1.2-4.6	923-4582	65 ; 15
0.9			11.2-56.4	2.8-14.1	1303-6164	Isothermal 22°C
						45 ; 15
						55 ; 15
				2.5-12.6	1296-5847	65 ; 15
1	30					Isothermal 22°C

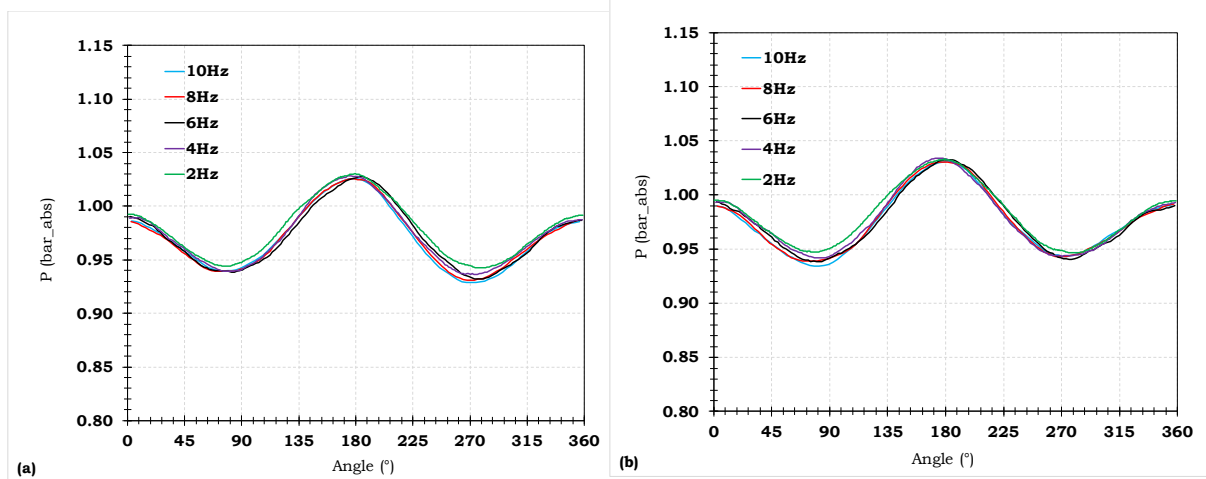*Table 4 : Test conditions for reciprocating flow. $Re_{dh,max}$ corresponds to the 30 mm stroke case.*

Figure 7: Pressure at both inlets (a): cold inlet P_C - (b): hot inlet P_H for an empty regenerator ε=1. *C*=30 mm - *freq* = 2-10 Hz – Isothermal flow (22°C)

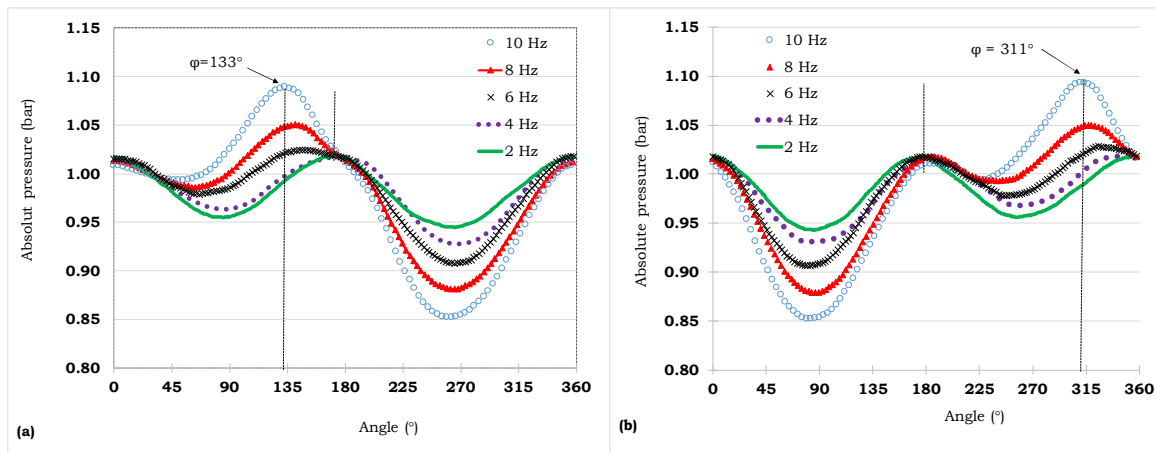
Figure 8: Pressure at the cold inlet P_C (a) and hot inlet P_H (b) for a regenerator ε=0.8. C=30 mm – Isothermal flow (22°C)

Figure 9 shows the velocity curves at both inlets of the regenerator as well as the theoretical speed of the piston for an isothermal flow, a porosity of ε=0.8 and a piston stroke of *C*=30 mm. As the velocity probes measure only absolute values, all the velocities are positive, thus the direction of flow is indicated on the graph. We observe a phase angle delay of about 22° between the actual velocities of the fluid and that of the piston. This angle shift may be explained by the inertia of the fluid. We also note that the upstream velocity is lower than the downstream one. This is due to the fact that the upstream pressure is higher than the downstream pressure. The influence of the frequency on the upstream velocity is plotted in Figure 10. The piston stroke is kept constant, therefore the velocity raises with the frequency. The phase angle increases with the frequency. At 2 Hz, the gas velocity appears to be in phase with the piston velocity, then at higher frequencies, the angular delay increases up to 22°. As inertial effects are 90° out of phase from viscous effects, we conclude that even at 10 Hz, the main reason from the increase in pressure is viscous effects or minor losses. We also observe that during the second half of the period, the velocity signal is smoother than in the first half. This is due to the presence of the flow straightener between the probe and the regenerator (Figure 5).
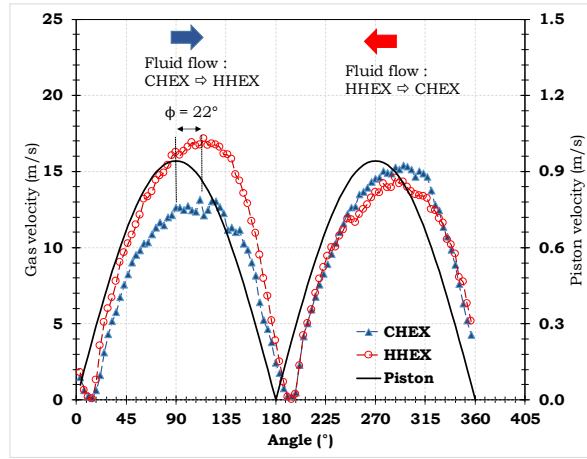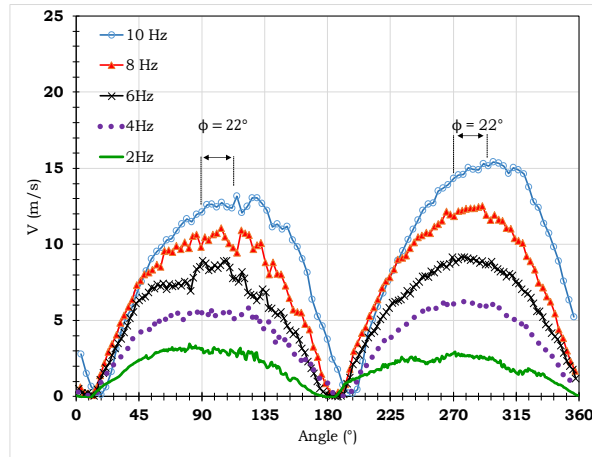
Figure 10: Gas velocity at the cold heat exchanger inlet for a regenerator ε=0.8. *C*=30 mm – Isothermal flow (22°C) – *freq* = 2-10 Hz

4.2 Pressure drop in isothermal and non-isothermal oscillating flow

We carried out isothermal flow tests at 22°C and followed by tests in the presence of thermal gradients of 30 °C, 40 °C and 50 °C in order to check the pressure drop in conditions closer to the real operation of a regenerator. The pressure drop ($\Delta P = P_C - P_H$) at isothermal conditions for a regenerator of porosity ε=0.8 and a piston stroke *C*=30 mm is plotted in Figure 11. We observe an increase in the pressure drop at higher frequencies. This pressure drop is probably mainly due to viscous effects as the velocity increases with frequency. We also observe a phase shift of the maximum pressure drop as the frequency raises (Figure 12) compared to the crank angle. For a frequency of 10 Hz ($Re_\omega = 18$), the phase shift is 22°. At 2 Hz, the pressure loss seems to be in phase with the crank angle. This phase shift may be due to inertial effects. As the applied thermal gradients cause a slight modification of 7 % in the fluid dynamic viscosity, we do not observe a significant variation between isothermal and non-isothermal curves (Figure 13).
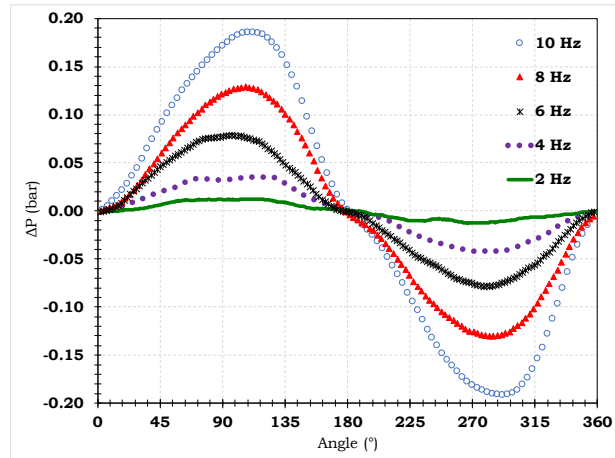
14

Figure 11: Pressure drop for a regenerator ε=0.8. *C*=30 mm – Isothermal flow – *freq* = 2-10 Hz
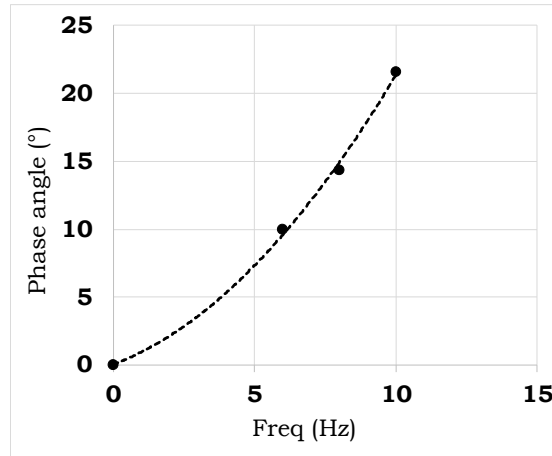

Figure 12: Maximum pressure drop phase angle shift versus frequency ε=0.8. *C*=30 mm – Isothermal flow – *freq* = 2-10 Hz
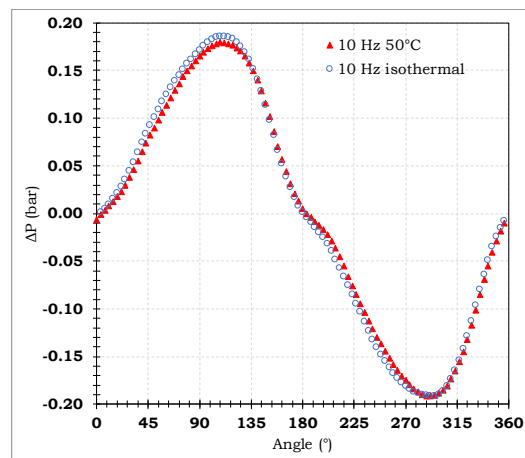

Figure 13: Pressure drop for a regenerator ε=0.8 - *C*=30 mm – Isothermal and temperature gradient flow – *freq* = 10 Hz

15

The influence of the porosity is plotted in Figure 14 for a piston stroke of 30 mm, a thermal gradient of 50°C and a frequency of 10 Hz. The amplitude of the pressure loss signal increases as porosity decreases. For a frequency of 10 Hz, the maximum pressure loss decreases by 81% for a porosity increase of 5% between 0.8 and 0.85 and of 26% between 0.85 and 0.9. Similar results were achieved for lower temperature gradients.
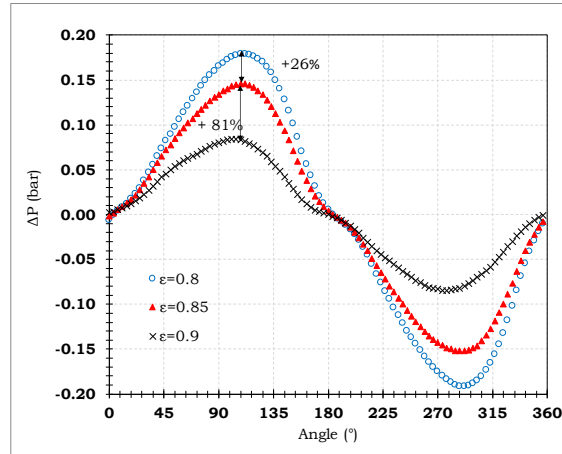

Figure 14: Pressure drop for a regenerator ε=0.8; 0.85; 0.9 - *C*=30 mm – ΔT=50°C – *freq* = 10 Hz

The influence of the piston stroke is plotted in Figure 15. Two strokes are analyzed: 24 and 30 mm. The porosity is 0.8 and the temperature gradient is 50°C. At a constant frequency, a longer stroke means a higher velocity, therefore we observe a higher pressure drop (+50%) for the longest stroke (+25 %). We also observe a small phase shift (≈6°) between the curves probably due to inertial effects.

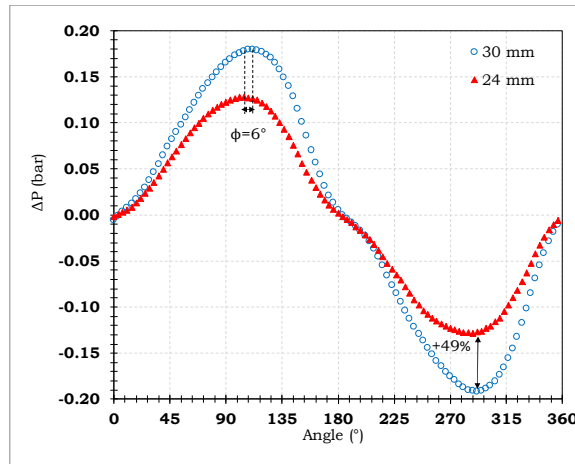Figure 15: Pressure drop for a regenerator ε=0.8. *C*=24 mm ; 30 mm —— ΔT=50°C – *freq* = 10 Hz

In order to compare the reciprocating flows and the steady flow performance of the regenerator, tests were conducted in unidirectional isothermal flows (Table 5). The maximum pressure drop over the cycles are plotted in Figure 16 versus $Re_{Dh,max}$. We observe a higher pressure drop in oscillating flow for the highest porosity 0.9. For lower porosities (0.85 and 0.8), we observe that the pressure drop is very close in oscillating and steady flow for a maximum Reynolds number lower than 5000, and Valensi

16

Hsu *et al*. [10] and Gedeon *et al.* [8] also observed a transition between a zone where the pressure losses are similar and another zone at higher Valensi number where the pressure losses are higher in oscillating flow. This increase may be due to inertial effects, local pressure losses or a change in the flow regime in steady and oscillating conditions.

Porosity	Flow rate (l/min)	Thermal condition
0.8		
0.85	0 - 50	Isothermal 22°C
0.9		

Table 5: Test conditions for a unidirectional steady flow
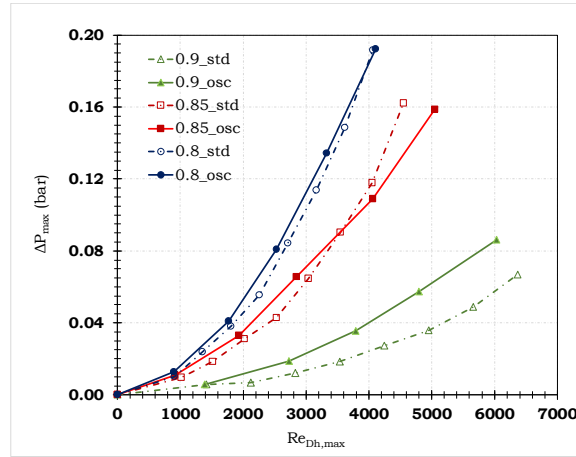

Figure 16: Comparison of the maximum pressure drop at steady state and oscillating flow. *freq* = 2-10 Hz ; ε=0.8-0.9 ; C=30 mm —— isothermal flow (22°C) – std denotes steady flow ; osc denotes oscillating flow

4.3 Friction factor

4.3.1 Instantaneous friction factor

The instantaneous friction factor $f(t, u(t), du/dt(t))$ is plotted in Figure 17 for a porosity of ε=0.8, a stroke *C*=30 mm in the isothermal case and for a frequency *freq*=10 Hz. The friction factor without the contribution of the inertial term $f(t, u(t))$ is also plotted on this graph. We observe that the instantaneous friction factor decreases from 0° to 180°, then from 180° to 360°. The inertial term does not significantly contribute to the friction factor. Similar results were achieved for a 0.85 and 0.9 porosity (Figure 19). Therefore, the difference in steady state unidirectional flow and oscillating flow observed in §4.2 cannot be explained only by the contribution of the acceleration in the frequency range 0-10 Hz.
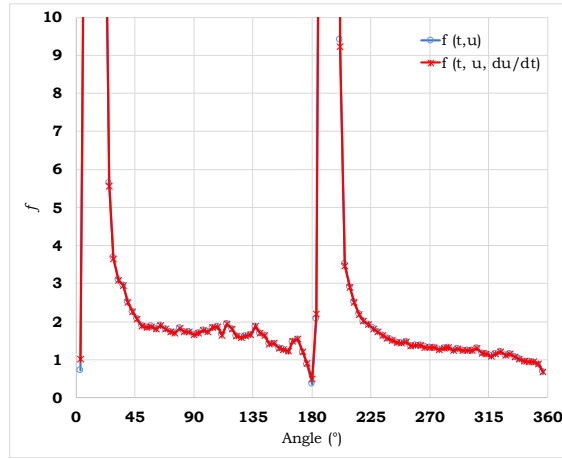
Figure 17: Instantaneous friction factor versus crank angle - ε=0.8; C=30 mm — isothermal – *freq* = 10 Hz

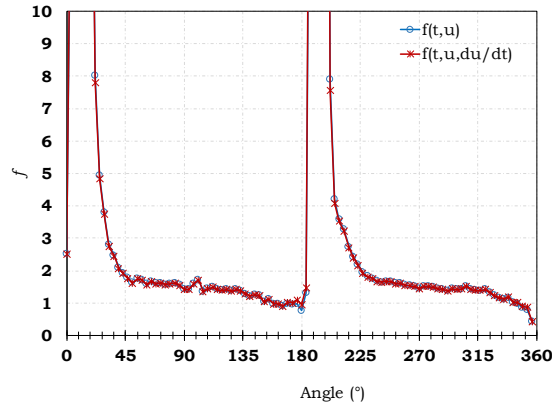Figure 18: Instantaneous friction factor versus crank angle - ε=0.9; C=30 mm — isothermal – *freq* = 10 Hz

The instantaneous friction factor is plotted versus the instantaneous Reynolds number in the discharge Figure 19(a) and suction phase Figure 19(b). We observe that the maximum Reynolds number is higher in the suction phase, as the velocity is higher in this phase. In the suction phase, the friction factor curve is smoother because of the presence of the flow straightener (Figure 5). The friction factor tends to a limit value as the Reynolds number tends to its maximum value. A similar behavior was observed for the other porosities.
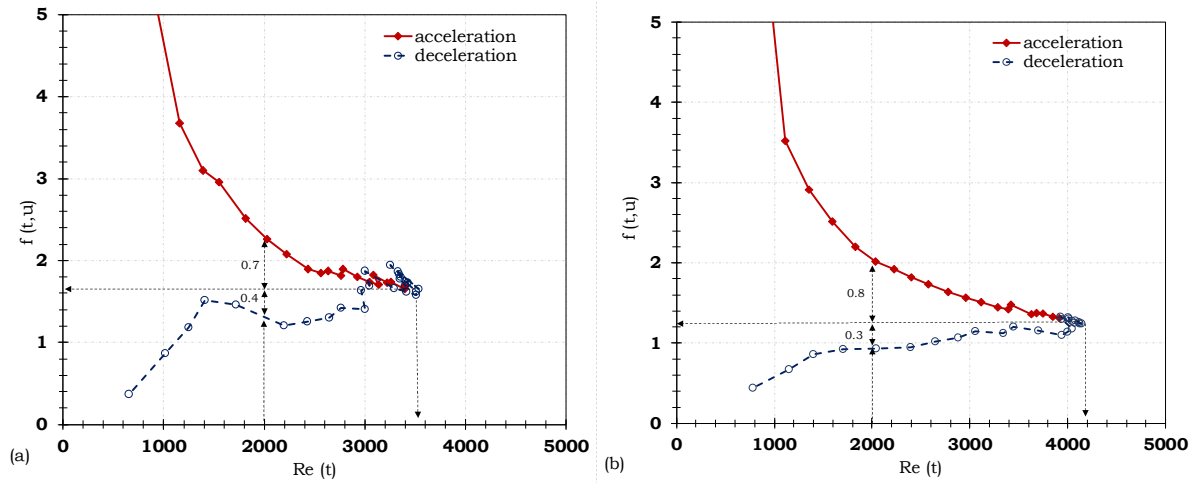
Figure 19: Instantaneous friction factor versus Reynolds number – (a) Discharge (b) Suction - ε=0.8; C=30 mm –– isothermal flow (22°C) – *freq* = 10 Hz

The friction factor limit, the observed deviations for the suction or discharge phases and the accelerating or decelerating phases are reported in

Table 6. In order to compare similar figures, the values all correspond to a Reynolds number of *Re*=2000 (Figure 19). We observe that the maximum Reynolds number increases as the porosity increases. The limit friction factor decreases as the porosity and maximum Reynolds number increase. This result is consistent with the works of Tanaka *et al.* [7], Zhao *et al.* [9] , Hsu *et al.* [10], and Leong *et al.* [12] on woven screens and open cell foam regenerators. The friction factor is clearly different in the acceleration and deceleration phases. It is higher than the limit factor in the acceleration phase and lower in the deceleration phase. This observation is consistent with Isshiki *et* al. [31] and Wang *et* al. [11] works for woven screens regenerators. This effect may be linked to the formation of eddy structures in the flow in the acceleration phase [31]. This formation dissipates energy in friction. In the deceleration phase, the structure are already formed therefore less energy is dissipated.

		Discharge		Suction	
		Acceleration	Deceleration	Acceleration	Deceleration
$\epsilon = 0.8$	$Re_{D_h,max}$	3500		4200	
	f_{limit}	1.7		1.3	
	Δf_{acc}	0.7	/	0.8	/
	Δf_{dec}	/	-0.4	/	-0.3
$\epsilon = 0.85$	$Re_{D_h,max}$	4200		5400	
	f_{limit}	1.6		1.2	
	Δf_{acc}	1	/	1.2	/
	Δf_{dec}	/	-0.4	/	-0.2
$\epsilon = 0.9$	$Re_{D_h,max}$	6000		6000	
	f_{limit}	1.4		1.4	
	Δf_{acc}	2.4	/	2	/
	Δf_{dec}	/	-0.4	/	-0.6

Table 6. Friction factors in the discharge and suction phases for different porosities

4.3.2 Comparison of the maximum friction factor in oscillating flow and the friction factor in steady flow

The maximum friction factor in oscillating flow and the friction factor in steady flow are plotted in Figure 20. We observe close values for the porosities 0.8 and 0.85. A significant difference appears for the highest porosities ($\epsilon = 0.9$). This result is consistent with the results obtained for pressure drop in §4.2.
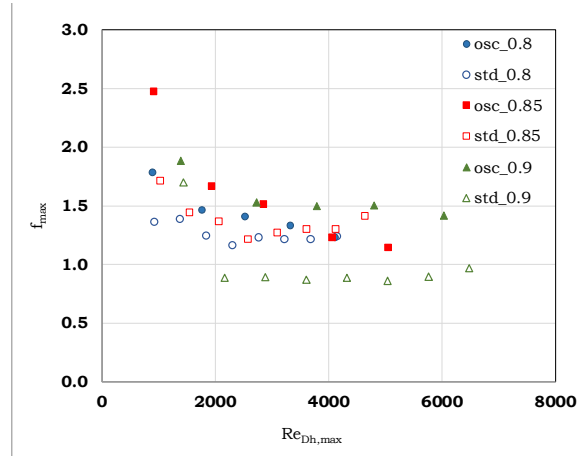

Figure 20: Comparison of the friction factor for oscillating and steady state flows. "std" denotes steady flow ; "osc" denotes oscillating flow

4.3.4 Determination of an experimental correlation for the maximum friction factor

From the different test results summarized in the Figure 21, we derive a correlation equation for the determination of the friction factor in a regenerator made from an array of pillars of lenticular shape, porosities varying from 0.8 to 0.9, maximum Reynolds number varying from 900 to 6300 and for an isothermal flow:

$$f = 11.88 Re_{D_{h,max}}^{-0.262} \tag{12}$$

This correlation was compared to existing correlations (Table 1) in the range of the maximum Reynolds numbers validity for the correlations. The results are plotted in Figure 22. We observe, as analyzed by Hsu *et al.* [10], that at low maximum Reynolds number, the friction factor of regenerators seems to tend to a Darcy limit where viscous effects dominate, and that at high maximum Reynolds number the friction factor seems to tend to a Forchheimer limit where inertial effects dominate. We observe that the friction factor amplitude reported for regenerators of various geometries are different: higher for metal felts (Gedeon and Wood [8]), lower for involute foils (Ibrahim *et al*. [14], Sun *et al.* [15]) and in between for woven screens and arrays of pillars, even if the porosities are comparable. The different geometries of the porous material lead to different flow fields and probably to a different transition to turbulence. These elements may explain these differences. At high maximum Reynolds number, the friction factor observed for our regenerator made from an array of pillars is similar to that calculated from Gedeon *et al.*'s correlation [8] for a woven screen regenerator.
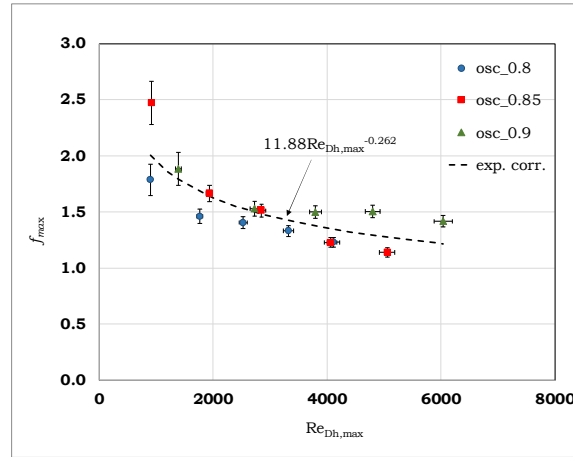
Figure 21: Maximum friction factor versus $Re_{D_h,max}$ – 900 < $Re_{D_h,max}$ <6000 - std denotes steady flow ; osc denotes oscillating flow
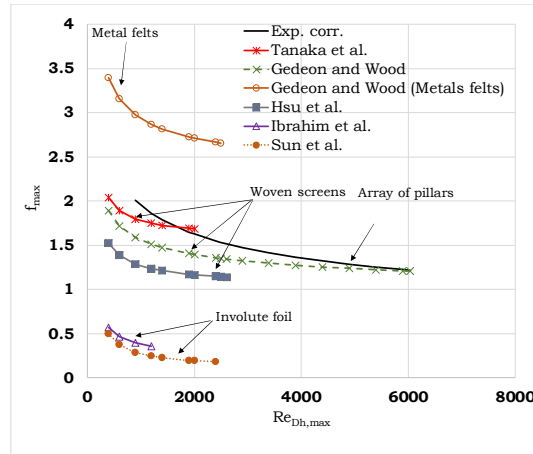

Figure 22: Comparison with existing correlations for the friction factor for various types of regenerators

5 Conclusion

In this paper, we present an experimental study on the pressure, pressure drop, velocity, and friction factor in a regenerator made from an array of pillars in reciprocating flow conditions. We show that the pressure drop depends on the porosity, frequency and piston stroke. We observe a phase shift between the crank angle sinusoidal variation of the piston and the pressure variation. This phase shift increases with frequency and may be due to inertial effects. The instantaneous friction factor is higher in the discharge phase than in the suction phase. It is also higher in the acceleration than in the deceleration phase. Friction factor in oscillating flow appears to be higher than friction factor in steady unidirectional flow for the highest porosity. For the lowest porosities, we observe that the pressure drop and friction factors are similar for maximum Reynolds numbers lower than 5000. An experimental correlation for the friction factor of the regenerator is derived in order to design a millimetric Stirling engine. The friction factor seems to tend to a Darcy limit where viscous effects dominate at low maximum Reynolds number, and at high maximum Reynolds number, the friction factor seems to tend to a Forchheimer limit where inertial effects dominate. The comparison of our experimental results

21

with existing correlations established for woven screen, metal felts and involute foil regenerators reveals that the <mark>amplitude</mark> of the regenerator friction factor lies in the same range as the friction factors of woven screens regenerators. However, significant differences appears in the friction factor trends at low maximum Reynolds number. Therefore, the experimental correlation established in this paper has to be used.

Funding

References

[1]   F. Formosa and L.G. Fréchette. Scaling laws for free piston Stirling engine design: Benefits and challenges of miniaturization. *Energy*, 57:796–808, 2013.

[2]   E. Dellali, S. Bégot, F. Lanzetta, E. Gavignet, R.K. Chutani, and J.Y. Rauch. Design, fabrication and CFD modeling of a Stirling engine microregenerator. In *17th International Stirling Engine Conference and Exhibition, 24th-26th August, Northumbria Univesity, Newcastle upon Tyne, UK*, pages 190 – 200, 2016.

[3]   I. Urieli and D.M. Berchowitz. *Stirling cycle engine analysis*. Bristol: Adam Hilger, 1984.

[4]   W.M. Kays and A.L. London. *Compact Heat Exchangers, 3rd*. NY: MacGraw-Hill Book Company, 1984.

[5]   H. Miyabe, K. Hamaguchi, and K. Takahashi. An approach to the design of Stirling engine regenerator matrix using packs of wire gauzes. In *Proc., Intersoc. Energy Convers. Eng. Conf.;(United States)*, volume 4, 1982.

[6]   G. Xiao, H. Peng, H. Fan, U. Sultan, and M. Ni. Characteristics of steady and oscillating flows through regenerator. *International Journal of Heat and Mass Transfer*, 108:309 – 321, 2017.

[7]   M. Tanaka, I. Yamashita, and F. Chisaka. Flow and heat transfer characteristics of the Stirling engine regenerator in an oscillating flow. *JSME international journal. Ser. 2, Fluids engineering, heat transfer, power, combustion, thermophysical properties*, 33(2):283–289, 1990.

[8]   D. Gedeon and J.G. Wood. Oscillating-flow regenerator test rig: hardware and theory with derived correlations for screens and felts. 1996.

[9]   T.S. Zhao and P. Cheng. Oscillatory pressure drops through a woven-screen packed column subjected to a cyclic flow. *Cryogenics*, 36(5):333 – 341, 1996.

[10]   Chin-Tsau Hsu, Huili Fu, and Ping Cheng. On pressure-velocity correlation of steady and oscillating flows in regenerators made of wire screens. *Journal of fluids engineering*, 121(1):52–56, 1999.

[11]   X. L. Wang, M. G. Zhao, J. H. Cai, J. T. Liang, and W. Dai. *Experimental Flow Characteristics Study of a High Frequency Pulse Tube Regenerator*, pages 439–444. Springer US, Boston, MA, 2005.

[12]   K.C. Leong and L.W. Jin. Characteristics of oscillating flow through a channel filled with open-cell metal foam. *International Journal of Heat and Fluid Flow*, 27(1):144 – 153, 2006.

[13]   M. Ibrahim, M. Wang, and D. Gedeon. Experimental investigation of oscillatory flow pressure and pressure drop through complex geometries. In *2nd International Energy Conversion Engineering Conference*, page 5560, 2004.

[14]   M. Ibrahim, S. Mantell D. Danila, T. Simon, S. Qiu G. Wood K. Kelly L. Sun, D. Gedeon, and J. McLean. A microfabricated segmented-involute-foil regenerator for enhancing reliability and performance of Stirling engines. Technical report, NASA/CR, 2007.

[15]   L. Sun, T. Simon, S. Mantell, M. Ibrahim, D. Gedeon, and R. Tew. Thermo-fluid experiments supporting microfabricated regenerator development for a Stirling space power engine. In *7th International Energy Conversion Engineering Conference*, page 4579, 2009.

[16]   M.P. Mitchell, D. Gedeon, G. Wood, and M. Ibrahim. Results of tests of etched foil regenerator material. *Cryocoolers*, 14:381–387, 2007.

[17]   M.T. Pamuk and M. Özdemir. Friction factor, permeability and inertial coefficient of oscillating flow through porous media of packed balls. *Experimental Thermal and Fluid Science*, 38:134 – 139, 2012.

[18]   M.S. Kahaleras, G. Layes, F. Lanzetta, and P. Nika. Friction factor and regenerator effectiveness in an oscillating gas flow. In *HTFFM 2014, Heat Transfer and Fluid Flow in Microscale*, apr 2014.

[19]   Y. Peles, A. Kosar, C. Mishra, C.J. Kuo, and B. Schneider. Forced convective heat transfer across a pin fin micro heat sink. *International Journal of Heat and Mass Transfer*, 48(17):3615–3627, 2005.

[20]   P.P.P. M. Lerou, G.C.F Venhorst, C.F. Berends, T.T. Veenstra, M. Blom, J.F. Burger, H.J.M Brake, and H. Rogalla. Fabrication of a micro cryogenic cold stage using mems-technology. *Journal of Micromechanics and Microengineering*, 16(10):1919, 2006.

[21]   C. Harris, K. Kelly, Tao Wang, A. McCandless, and S. Motakef. Fabrication, modeling, and testing of micro-cross-flow heat exchangers. *Journal of Microelectromechanical Systems*, 11(6):726–735, Dec 2002.

[22]   S. Srinivas, A. Dhingra, H. Im, and E. Gulari. A scalable silicon microreactor for preferential co oxidation: performance comparison with a tubular packed-bed microreactor. *Applied Catalysis A: General*, 274(1):285 – 293, 2004.

[23]   P.V. Trevizoli, A.T. Nakashima, G.F. Peixer, and J.R. Barbosa. Performance assessment of different porous matrix geometries for active magnetic regenerators. *Applied Energy*, 187:847 – 861, 2017.

[24]   S. Vanapalli, H.J.M. Brake, H.V. Jansen, J.F. Burger, H.J. Holland, T.T. Veenstra, and M.C. Elwenspoek. Pressure drop of laminar gas flows in a microchannel containing various pillar matrices. *Journal of Micromechanics and Microengineering*, 17(7):1381, 2007.

[25]   T.M. Jeng, S.C. Tzeng, W.T. Hsu, and G.W. Xu. Flow visualization and heat transfer characteristics of oscillating fluid through pin-fin array in a rectangular channel. *Advances in Mechanical Engineering*, 5:283830, 2013.

[26]   I. Rühlich and H. Quack. *Investigations on Regenerative Heat Exchangers*, pages 265–274. Springer US, Boston, MA, 2002.

[27]   S.G. Kandlikar and W.J. Grande. Evolution of microchannel flow passages: thermohydraulic performance and fabrication technology. In *ASME 2002 International Mechanical Engineering Congress and Exposition*, pages 59–72. American Society of Mechanical Engineers, 2002.

[28]   F. Lanzetta and E. Gavignet. Thermal measurements and inverse techniques, part. 1 chap 3-temperature measurements: Thermoelectricity and microthermocouples, 2011.

[29]   Evaluation of measurement data. Guide to the expression of uncertainty in measurement JCGM 100:2008 (GUM 1995 with minor corrections). Technical report, 1995.

[30]   D.S. Arnold, A. Tura, and A. Rowe. Experimental analysis of a two-material active magnetic regenerator. *International Journal of Refrigeration*, 34(1):178 – 191, 2011.

[31]   S. Isshiki, Y. Takasaki, and I. Ushiyama. An experimental study on flow resistance of regenerator wire meshes in oscillatory flow. In *Energy Conversion Engineering Conference, 1997. IECEC-97., Proceedings of the 32nd Intersociety*, 1997.